ChemElectroChem

Research Article
doi.org/10.1002/celc.202300111

Chemistry Europe
European Chemical Societies Publishing

www.chemelectrochem.org

Controlling the Reactivity and Interactions between Hydrogen and Palladium Nanoparticles via Management of the Particle Diameter

Lilian Moumaneix, Akseli Rautakorpi, and Tanja Kallio*[a]

Tailoring the interactions between hydrogen and palladium is crucial for numerous industrial and research applications. The fine control of Pd nanoparticles (NPs) diameter is promising to address this problem when other means, i.e. temperature, pressure, or cell voltage, are set by the ongoing process. We investigate the electrochemical behaviour of Pd NPs in the presence of hydrogen over a large range of particle diameters, between 3.8–21.5 nm. The study is carried out in both a three-electrode setup and a proton pump. A linear relationship between the H/Pd ratios and the NPs diameter is evidenced. The increase in particle size is accompanied by an extension of the loading duration to reach a stable hydride. Beyond H absorption, the HER and HOR kinetics are examined as a function of the particle diameter. The smaller the particle the higher the catalytic activity, with exchange currents ranging between approx. 1.7–9.8 mA mg_{Pd}^{-1}.

Introduction

The peculiar behaviour of hydrogen atoms when in contact with palladium has attracted worldwide attention, from fundamental studies to applications in hydrogen purification, hydrogen sensors or hydrogen storage.[1–5] Another promising usage of palladium, and more specifically of palladium hydrides, is related to its catalytic activity for various reactions, e.g. hydrogenation of alkynes into alkenes,[6–9] CO_2 reduction,[10] or nitrogen reduction reaction.[11,12] The accurate control of the hydrogen concentration in PdH_x systems is of primordial importance as many of its properties may vary with x, e.g. electrical, magnetic, or mechanical properties.[13] In the field of catalysis, the concentration of H in Pd can greatly affect the selectivity of the material towards a specific reaction product.

The chemical process leading to the insertion of hydrogen into the Pd structure has been thoroughly documented in the literature.[14,15] In brief, protons undergo adsorption on the Pd surface according to the Volmer equation (eq. 1), followed by the subsequent diffusion of the adsorbed species to subsurface positions (eq. 2)[16] and bulk positions (eq. 3).[15] Alternatively, adsorbed hydrogen atoms can react and form gaseous dihydrogen, following an electrochemical (eq. 4) or non-electrochemical (eq. 5) desorption route.

$$H^+ + Pd + e^- \rightleftarrows PdH_{ads} \quad (1)$$

$$PdH_{ads} + Pd_{sub} \rightleftarrows Pd_{surface} + PdH_{sub} \quad (2)$$

$$PdH_{sub} \rightleftarrows PdH_{abs} \quad (3)$$

$$PdH_{ads} + H^+ + e^- \rightleftarrows Pd + H_2 \quad (4)$$

$$2PdH_{ads} \rightleftarrows 2Pd + H_2 \quad (5)$$

Palladium hydrides have been widely studied for their catalytic properties for many reactions of interest. In the petrochemical industry, PdH_x is used to convert alkynes into alkenes through a partial hydrogenation reaction. The catalytic activity and selectivity of PdH_x for this reaction have been directly linked to the number of H atoms introduced in the Pd structure. The α-PdH_x phase ($x < \approx 0.05$) presents a higher selectivity but lower reaction rate than the β-PdH_x phase ($x > \approx 0.6$)[17,18,9] This result is due to the direct participation of the hydrogen atoms located in the subsurface layers of Pd in the hydrogenation reaction.[6–8]

Palladium also exhibits good properties for the preparation of syngas from the reduction of CO_2 in acidic media. In the common operating voltage range, ca. −0.5–−1.0 V, the palladium transformation into PdH prevents surface poisoning by adsorbed CO, as is the case with Pt.[10] Furthermore, palladium hydride has demonstrated enhanced catalytic activity for the nitrogen reduction reaction compared to metallic palladium due to the presence of H atoms in the Pd lattice which are actively involved in the reduction reaction.[11,12]

Controlling the number of H atoms in PdH_x can be achieved in different ways, taking advantage of the sensitivity of this system to H_2 pressure,[19,20] temperature,[21,22] or electric voltage. Electrochemical means have been proven to be especially suitable and easy to use to control the H absorption by choosing an adequate potential range.[23–27] These three parameters have been extensively reported in the literature, and their

[a] Dr. L. Moumaneix, A. Rautakorpi, Prof. T. Kallio
Department of Chemistry and Materials Science, School of Chemical Engineering, Aalto University, 00076 Aalto, Finland
E-mail: tanja.kallio@aalto.fi
Homepage: https://research.aalto.fi/en/persons/tanja-kallio

Supporting information for this article is available on the WWW under https://doi.org/10.1002/celc.202300111

influence on H absorption is quite well-known and understood. However, in some cases, the desired application does not allow the modification of one or several of these parameters. Hence, another way of adjusting the hydrogen absorption in Pd can be attained by controlling the palladium morphology, e.g. nanoparticle (NPs) size or thin film thickness.

For Pd thin films, the maximal absorption of H into Pd strongly depends on the film thickness. When reported in terms of H/Pd ratio, the H absorption decreases as the film gets thicker.[28] Authors suggest that a high concentration of H is located in a Pd sublayer, contributing greatly to the overall H absorption. Thinner films may have smaller crystallites, therefore more grain boundaries, where most of the H atoms would be located.[28]

In the case of Pd NPs, the absorption mechanism is quite different as it does not involve grain boundaries. It has been proposed that Pd NPs present a core-shell structure, in which the lattice parameter of the core is close to the one of bulk Pd, whereas that of the shell is larger.[5] The absorption of hydrogen is usually lower in NPs than in bulk Pd, and more generally, the maximum absorption increases with the NPs size. The larger H/Pd ratios observed for large NPs may be due to the decreasing enthalpy and entropy of formation of palladium hydride with the increase in particle size, correlated with the decreasing compression strain at the interior of the NPs due to the curvature of the free surface.[29] It is commonly admitted that the solubility of H atoms in the α-PdH phase is enhanced as the NPs size decreases, whereas the sorption capacity in the β-PdH phase decreases.[5,9] Confirming this behaviour, Ingham *et al.* reported X-ray diffraction results displaying clear trends of the increase in the α-PdH and decrease of the β-PdH lattice parameters along with the decrease in NPs size.[20] In addition to the NPs size, the state of aggregation and the nature of the surface can also affect hydrogen absorption.[9,20]

In this paper, the focus is put on investigating the electrochemical behaviour of Pd NPs as a function of the Pd nanoparticle size, in the range of 3.8–21.5 nm. Hydrogen insertion into Pd is studied under a large potential range, in a three-electrode setup, i.e. rotating disk electrode (RDE), as well as in a proton pump setup. Rarely used in the literature, proton pumps allow to carry out electrochemical measurements at lower potentials than typical liquid-electrolyte setups, due to the easy removal of H_2 evolved in the cathodic compartment, as well as mimic real application devices. Cell voltages up to −0.5 V are investigated, as compared to −0.1 V_{RHE} for the RDE setup. In addition to that, we report an investigation of the hydrogen evolution reaction (HER) and hydrogen oxidation reaction (HOR) kinetics via the fitting of experimental data with the Butler-Volmer equation. The influence of the presence or absence of Pd hydride on the reaction kinetics is also discussed.

Results and discussion

Physico-chemical analysis of the Pd NPs

The particle size distribution, shape, and level of aggregation of the Pd NPs deposited on Vulcan XC-72 were analysed using TEM (Figure 1(a–c)). By adjusting the synthesis parameters, i.e. the water-to-surfactant molar ratios, the NPs size distributions were controlled, and three samples were prepared. After fitting the experimental data with a normal distribution, the mean diameters of the Pd NPs were determined to be around 11.2 ± 3.2 nm, 17.1 ± 2.8 nm, and 21.5 ± 3.2 nm (Figure 1(d–f)). Additionally, a commercial material (Premetek, 20 wt-% Pd on Vulcan XC-72, 3.8 ± 0.6 nm, cf. S.I. 2) has been used as a reference throughout the paper. Thereafter, the samples are denoted *Pd NPs "S"*, *"M"*, *"L"*, and *Com* respectively. No significant aggregation of the Pd NPs was observed for any of the samples, even if this fact has to be nuanced as TEM is a local analysis. The aspect ratio of the Pd NPs was consistently measured to be around 1 (spherical).

The thermogravimetric analysis shows similar behaviours for the three samples (cf. Figure 2): (i) a first rapid mass loss starting at around 450–525 °C followed by (ii) a second mass loss between 570–600 °C, both corresponding to the combustion of the carbon phase; (iii) a slight increase in the mass of the samples above 650 °C, attributed to the oxidation of Pd into PdO. The presence of two successive mass losses might be related to the heterogeneous distribution of the Pd NPs on the Vulcan. Indeed, it is highly probable that the Pd NPs catalyse the combustion of the nearby carbon phase, resulting in an early decomposition, the first observed on the thermograms. In the case of areas with a lower concentration of Pd NPs, the combustion of the carbon phase could be delayed, occasioning a second mass loss.

The loading of Pd NPs on Vulcan was determined from the thermograms, assuming a total conversion of Pd into PdO. This assumption had been tested with the commercial catalyst powder, for which we obtained a loading of 21.7 wt-% Pd, i.e. 25.0 wt-% PdO. Table 1 gathers the characteristics of the three tested samples.

Table 1. Physico-chemical characteristics of the studied materials.

Sample ID	Mean particle size [nm]	Pd loading [wt.%]
Pd NPs Com	3.8 ± 0.6	21.7
Pd NPs "S"	11.2 ± 3.2	18.7
Pd NPs "M"	17.1 ± 2.8	15.4
Pd NPs "L"	21.5 ± 3.2	14.3

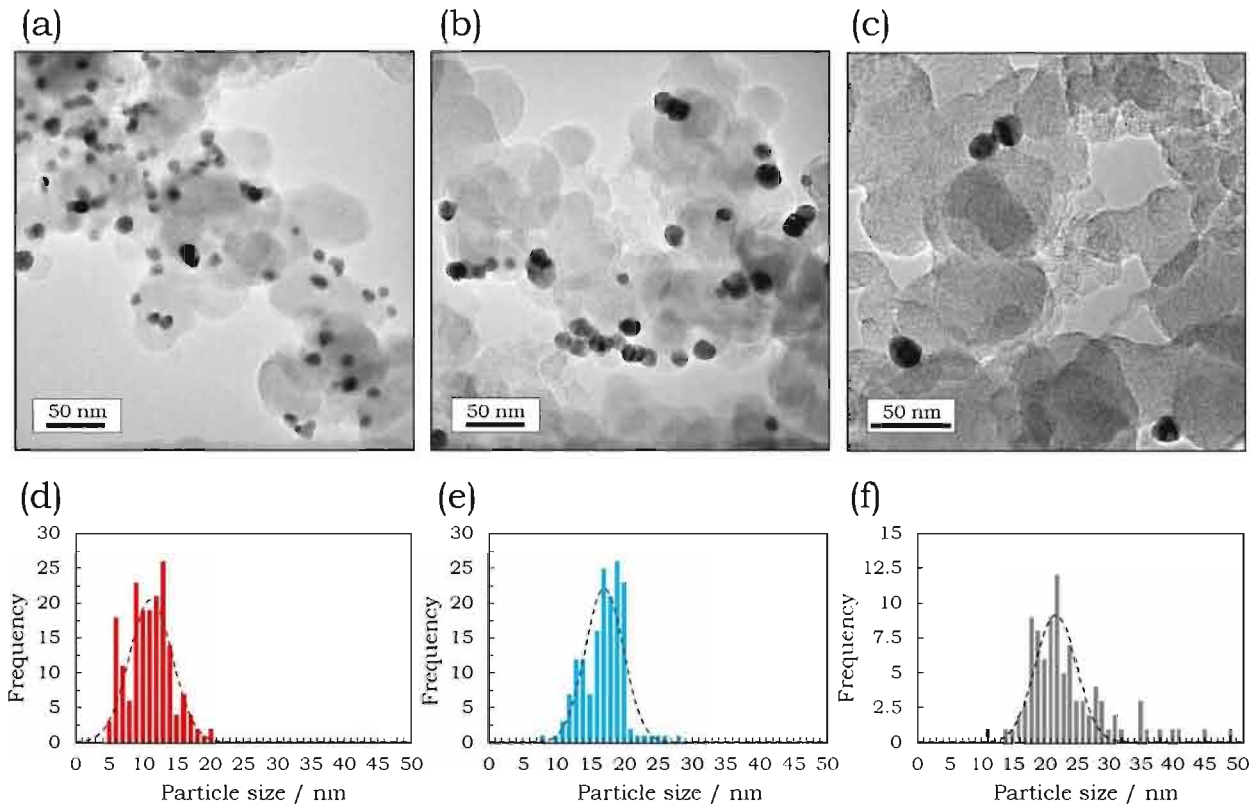

Figure 1. Typical micrography of the three prepared samples (a) Pd NPs "S" (11.2 ± 3.2 nm), (b) Pd NPs "M" (17.1 ± 2.8 nm) and (c) Pd NPs "L" (21.5 ± 3.2 nm). Particle size distributions of (d) Pd NPs "S" (180 particles), (e) Pd NPs "M" (165 particles) and (f) Pd NPs "L" (92 particles). The dotted lines correspond to the normal distribution fittings.

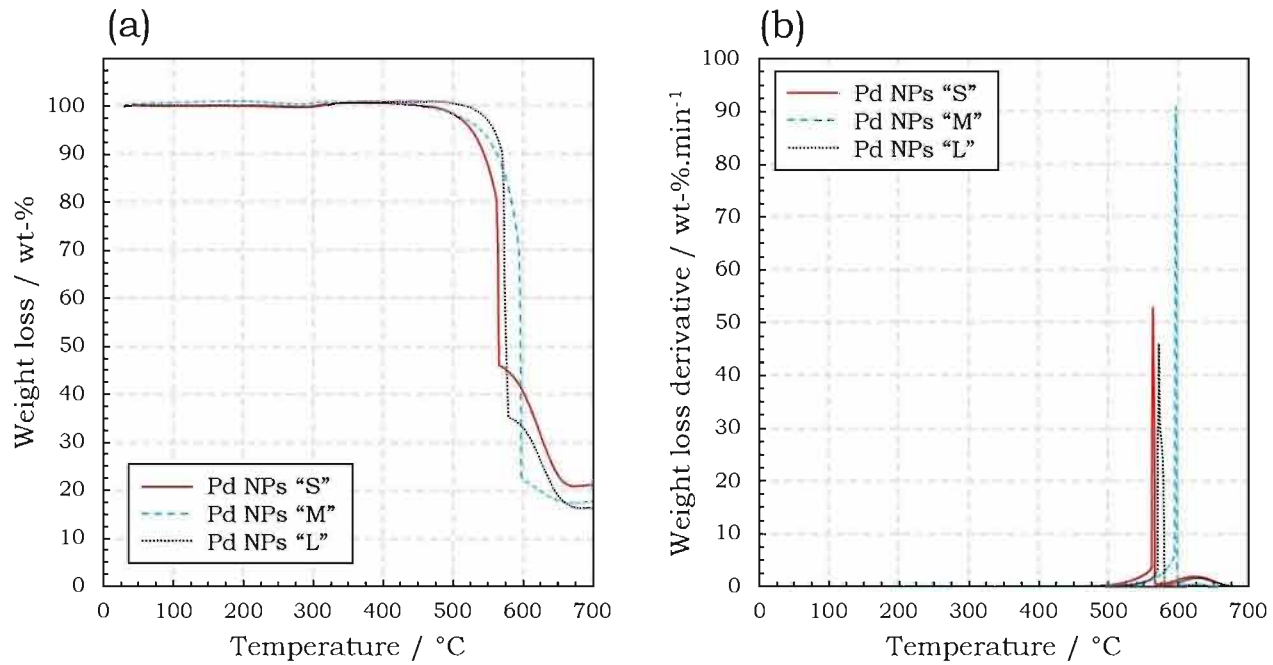

Figure 2. Thermograms (a) and weight loss derivatives (b) for the samples Pd NPs "S", "M" and "L". The TGA was operated under air, at a heating rate of 5 °C min^{-1}.

Influence of the NPs size on the interactions between hydrogen and palladium

Proton pump setup

As was already reported in earlier works,[22,23,24,27,32] the H insertion into Pd follows a two-plateau trend in regard to the loading cell voltage (Figure 3(a)). The plateau at high voltages, i.e. above 0.05 V, corresponds to the formation of the α-PdH phase, H/Pd <0.05, while the one at low voltages indicates the formation of the H-rich β-PdH phase. As the voltage is changed from $+0.3$ V to -0.5 V and back, a hysteresis appears as H desorption requires slightly higher voltages than H absorption, likely due to the structure of the Pd hydride, i.e. strains, plastic deformation during the hydride formation or change in the arrangement of H atoms inside the metal.[22,33,34]

The Pd NPs size displays a very strong influence on the insertion and desorption of H atoms into Pd. The maximum H/Pd ratio measured at -0.5 V increases with the NPs size, from 0.32 to 0.45 and 0.56 for *Pd NPs "S"*, *"M"*, and *"L"* respectively. These results are in accordance with Ingham *et al.* who reported maximum values of about 0.36, 0.28 and 0.12 for NPs of 6.1, 3.0 and 1.7 nm, respectively.[20] In the meantime, the number of H atoms dissolved in the α-PdH phase measured at 0.05 V decreases with the increase in the NPs size, from 0.06 to 0.05 and 0.04 for *Pd NPs "S"*, *"M"*, and *"L"* respectively. This result is in good agreement with the literature, as the solubility of H in the α-PdH phase is expected to increase with decreasing NPs size, while the H sorption capacity in the β-PdH phase is expected to decrease.[5,29,35] The observed behaviour is typical of Pd NPs, whereas an opposite trend is expected for Pd thin films. Gabrielli *et al.* suggest that in the case of thin films, grain boundaries might play an important role as H traps in Pd thin films, which are commonly not present in Pd NPs.[15,28] The authors also claim that a sublayer rich in H atoms contributes greatly to the global H/Pd ratio in thin films. Some studies describe Pd hydride in NPs as a core-shell structure, in which the outer shell, i.e. the subsurface, would present interstitial sites less favourable for the H absorption than the ones of the inner core.[35] In such a case, the number of interstitial sites suitable for H absorption decreases with the Pd NPs diameter, which would explain the opposite trend observed. Additional behaviours can also be discerned with increasing NPs size: (i) a slight opening of the hysteresis insertion/disinsertion, (ii) a shift of the transition between the α-PdH and β-PdH phases towards lower voltages, and (iii) a slightly slower transition between

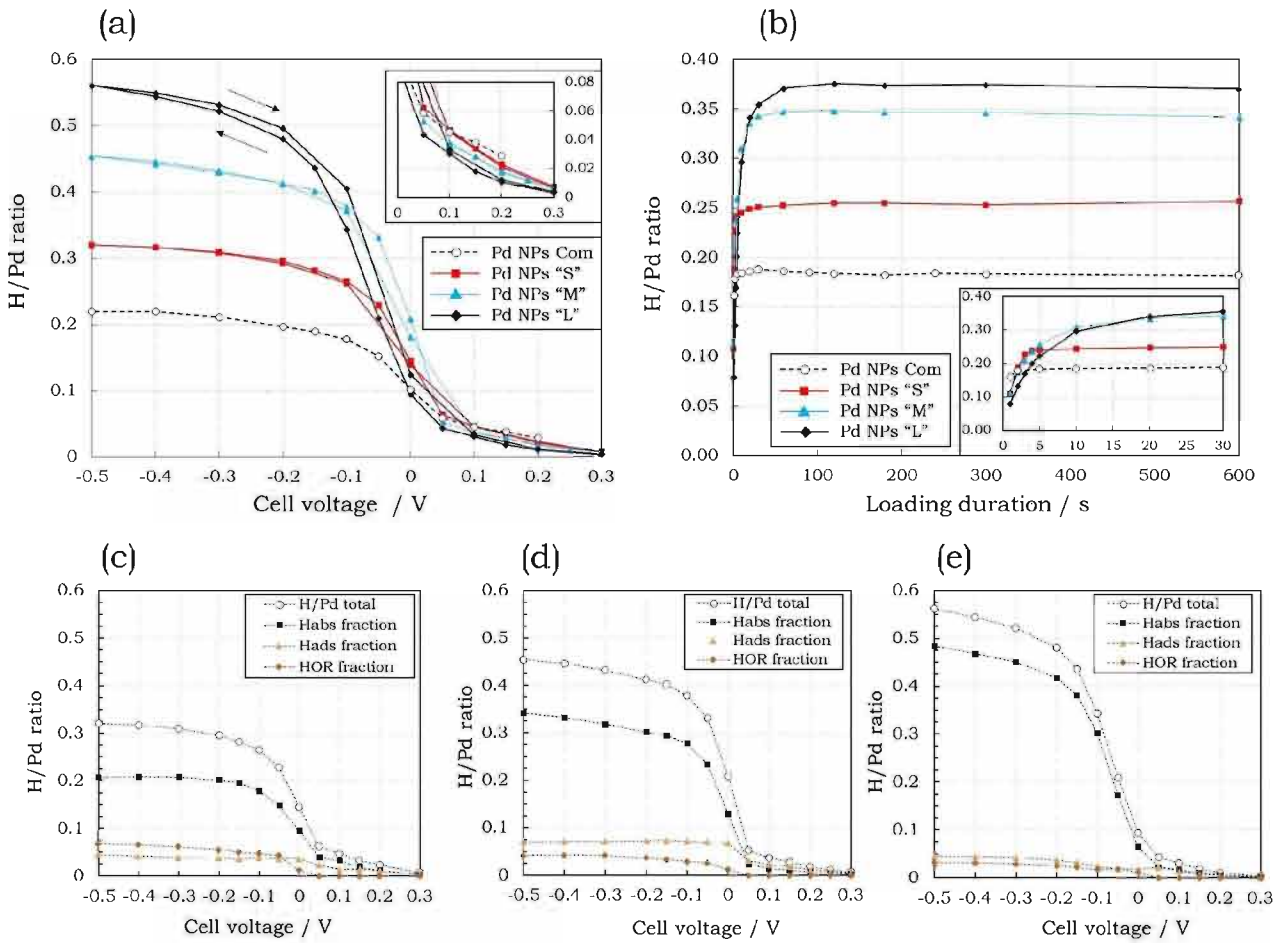

Figure 3. Cell voltage dependency (a) and loading duration dependency (b) on the H/Pd ratio measured from the electrochemical desorption curves. Separation of the different H fractions participating to the H/Pd ratio according to [23], Pd NPs "S" (c), Pd NPs "M" (d) and Pd NPs "L" (e). H_2 and N_2 flowrates 50 mL.min^{-1}, 30 °C, 120 s loading duration (a, c, d, e), -0.1 V loading voltage (b), desorption at $+0.4$ V for 120 s.

these two same phases. All these observations are in accordance with the literature.[20,29]

The electrochemical desorption curves (available in S.I. 2) were modelled using a procedure we reported in a previous publication.[23] Briefly, the model is based on the diffusion of different hydrogen species to the surface of Pd particles and their subsequent desorption in the form of protons and electrons through either the Volmer and/or Heyrovsky reactions. We refer the reader to this study for more information on the procedure. The curves presented in Figure 3(a) were decomposed into three contributions (Figure 3(c–e)): (i) the desorption of hydrogen atoms initially absorbed into the Pd NPs (H_{abs} fraction), (ii) the desorption of hydrogen atoms initially adsorbed on the Pd surface (H_{ads} fraction), and (iii) the oxidation of H_2 initially in the surroundings of the catalyst layer (*HOR* fraction). The model gives some insight into H absorption values closer to reality, as compared with a simple integration of the area under the desorption curve, due to the presence of additional contributions which are, in the latter case, neglected. As a confirmation of an earlier statement, the contribution from H_{abs} at −0.5 V increases with the NPs size, from about 0.21 to 0.34 and 0.48 for *Pd NPs "S"*, *"M"*, and *"L"* respectively. A decrease in the H_{ads} contribution would be expected with the increase in the NPs size, as the specific surface of the particles decreases with their diameter. However, the calculated H_{ads} at −0.5 V are quite consistent for the three samples, most likely due to the error margin of the model. Lastly, the *HOR* contribution, present at 0 V and below, shows a slightly faster increase for *Pd NPs "S"* compared to *Pd NPs "M"* and *"L"*, which might be related to the higher catalytic activity of small NPs towards the formation of H_2.

Finally, the influence of the loading duration on the H absorption was examined. As reported in an earlier study,[23] the loading of hydrogen atoms into Pd NPs is a very fast process. In Figure 3(b), it is possible to notice that the time necessary to reach an equilibrium state strongly depends on the NPs size. If the saturation of *Pd NPs "S"* is attainted in approximately 5 s, it takes about 30 s for *Pd NPs "M"* and 60–120 s for *Pd NPs "L"*. These results can be easily understood as the time for a hydrogen atom on the Pd surface to diffuse to the centre of the NPs is likely proportional to the size of the NPs. Additionally, once at equilibrium, longer loading durations do not seem to further enhance the H absorption. Similar trends were reported for Pd thin films, for which increasing the film thickness extended the time to reach saturation from a few seconds to a few hours.[25,36]

Three-electrode setup

The measurements carried out in the RDE setup show trends similar to the ones described for the PP (cf. Figure 4). The H/Pd are notably higher in the RDE setup, from 0.34 to 0.63 for *Pd NPs Com* and *"L"* respectively. This is likely due to the N_2 flushing the PP cathodic compartment, contributing to the increase in the H desorption rate, i.e. non-electrochemical removal (eq. 5), from the cathode catalyst layer. The number of H atoms involved in the α-PdH phase does not vary significantly for the three synthesized materials (cf. insert Figure 4(a)), whereas the Pd NPs Com exhibits larger values, as observed previously in the PP. No apparent reason for this discrepancy can be given at the moment.

The separation of the H/Pd ratios into H_{abs}, H_{ads}, and *HOR* fractions from the modelling of the desorption curves (available in S.I. 3) confirms the increase in H_{abs} along with the particle diameter, from approximately 0.27 for *Pd NPs "S"* to 0.42 for *Pd NPs "L"* at −0.1 V_{RHE}. The contribution coming from H_2 oxidation is consistent between the samples, likely due to the impossibility to store large quantities of H_2 around the WE because of its constant rotation. Surprisingly, the H_{ads} contribution increases slightly with the increase in particle diameter, from 0.10 for *Pd NPs "S"* to 0.16 for *Pd NPs "L"* at −0.1 V_{RHE}. This behaviour might be related to the higher HER reaction rate of small NPs compared to larger ones (cf. section 3.2.), shifting the equilibrium existing between H_{ads} and H_2 (eq. 4, 5) towards the formation of H_2. An extensive analysis would be necessary to determine if this trend is significant or due to an imprecision of the model.

As a summary, Figure 4(e) gathers the maximal H/Pd ratios reported in both electrochemical setups. It appears that in the investigated diameter range of 3.8–21.5 nm, the H/Pd ratios have a linear dependency on the particle diameter. Both setups display the same trend, the PP exhibits lower values, likely due to the N_2 flushing the cathodic compartment.

Influence of the NPs size on the electrochemical activity

Proton pump setup

The electrocatalytic activity towards HOR/HER of the samples was examined using linear sweep voltammetry (LSV). LSV was performed between the open circuit voltage (OCV) and a cell voltage low enough to observe the limit current, i.e. between −0.4 V and −0.6 V, at a scan rate of 2 mV s^{-1} (cf. Figure 5(a)). An enhancement of the mass activity of the catalyst materials can be witnessed as the particle size decreases, as could be expected from the literature.[37] Measured at 10 mA mg_{Pd}^{-1}, the onset voltage for the hydrogen absorption and HER increases from approximately 41 mV for *Pd NPs "L"* to 56 mV for *Pd NPs "S"*. The reference material displays an even higher onset potential, around 74 mV.

Cyclic voltammetry performed in the range from −0.1–0.4 V (before iR correction) shows large variations induced by the NPs sizes. In Figure 5(b), three peaks are evidenced: (i) hydrogen desorption from absorbed positions (thereafter noted H_{abs}), at 0.09 V, 0.11 V, 0.13 V and 0.19 V for *Pd NPs COM*, *"S"*, *"M"*, and *"L"* respectively (anodic scan), (ii) hydrogen desorption from surface positions (thereafter noted H_{ads}) around 0.25 V (anodic scan), and (iii) hydrogen adsorption around 0.22 V (cathodic scan). In addition to that, hydrogen absorption and hydrogen evolution occur at cell voltages below 0.05 V.

The desorption of H_{abs} shifts towards higher voltages as the particle size increases, which may be attributed to slower H

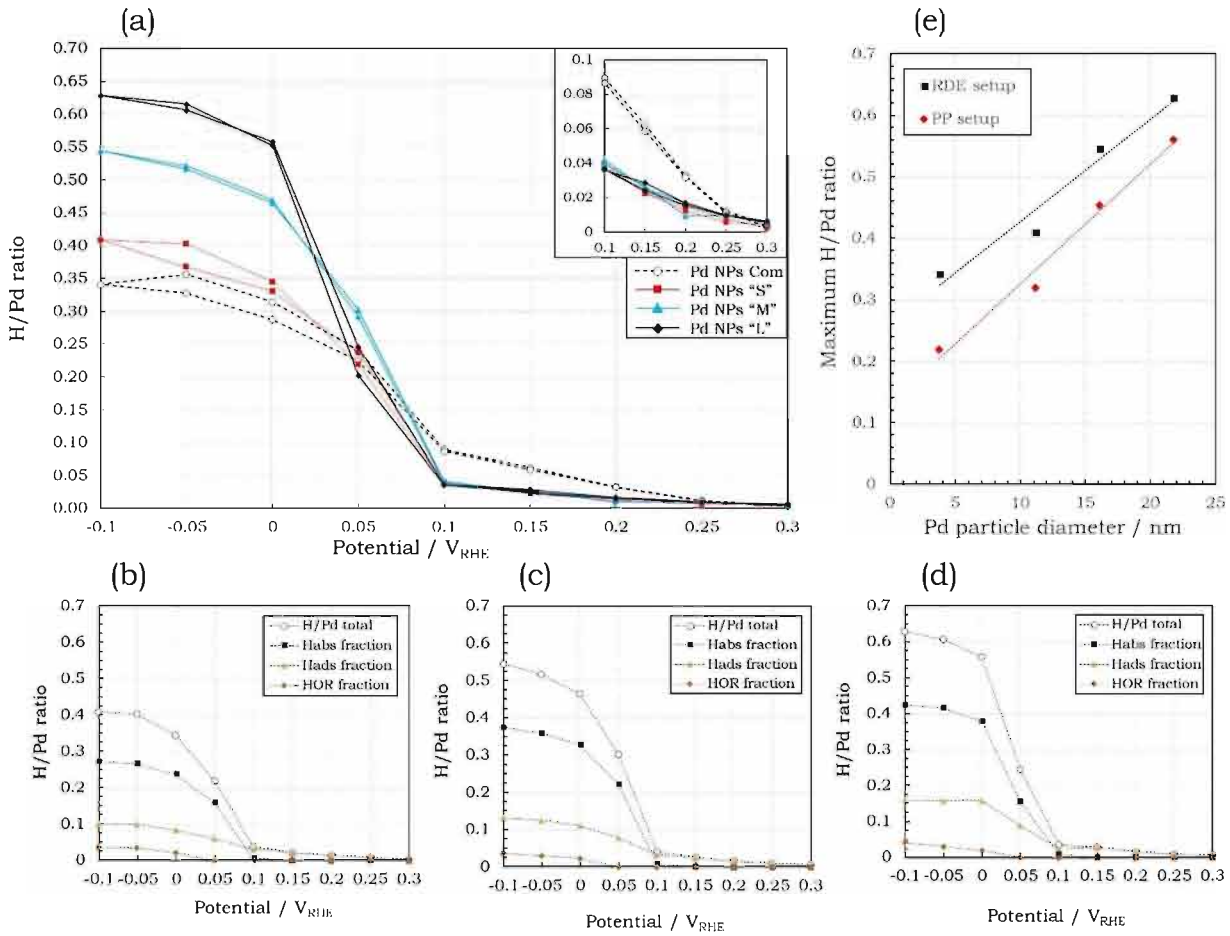

Figure 4. Potential dependency of the H/Pd ratio measured from the electrochemical desorption curves in the RDE setup (a). Separation of the different H fractions participating to the H/Pd ratio according to [23], Pd NPs "S" (b), Pd NPs "M" (c) and Pd NPs "L" (d). H_2SO_4 0.5 M, 25 °C, N_2 bubbling, 120 s loading duration, desorption at +0.4 V for 120 s. Particle diameter dependency of the H/Pd ratios measured at −0.1 V_{RHE} (RDE setup) and at −0.5 V (PP setup) (e).

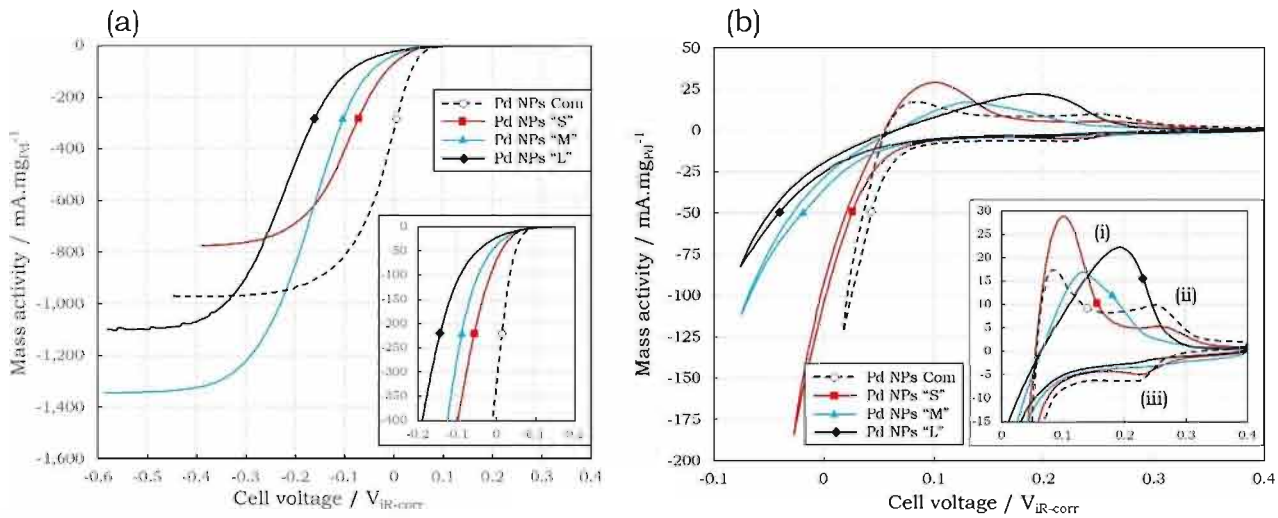

Figure 5. Linear sweep voltammograms recorded at 30 °C, with an H_2 and N_2 flowrates of 50 mL min^{-1}, at a scan rate of 2 mV s^{-1} (a); cyclic voltammograms recorded at 30 °C, with an H_2 and N_2 flowrates of 50 mL min^{-1}, at a scan rate of 25 mV s^{-1} (b). All voltages are iR-corrected.

diffusion rates from the large NPs compared to the smaller ones. Additionally, the current resulting from H_{ads} desorption and adsorption greatly decreases with the increase of the NPs diameter, which is likely related to a decrease in the specific

surface area, i.e. the surface-to-volume ratio decreases from 0.53 to 0.28 for the NPs of 11.2 nm and 21.5 nm of diameter respectively. Finally, the fraction of H_{abs} involved during the desorption process, i.e. the area under peak (i), seems to increase with the increase in particle size, which has been discussed thoroughly in the previous section.

Electrochemical impedance spectroscopy was performed in the range of −0.5–0.1 V to study the variation of the charge transfers on the anode (Pt) and cathode (Pd) sides, the ohmic resistance, and the mass transfer resistance under different operating conditions. The Nyquist plots are available in S.I. 4. Collected data were modelled with a modified Randles model composed of an ohmic resistance R_{ohm} in series with two identical subcircuits, both containing a resistance R_{ct} (charge transfer resistance) in parallel with a constant phase element. An additional resistance R_{mt} (mass transfer resistance) in parallel with a capacitor C_{mt} were added to model the mass transfer contribution appearing at low voltages. Using the circuit description code proposed by Boukamp,[38] the equivalent circuit can be written: R_{ohm} ($R_{ct,a}$ CPE_a) ($R_{ct,c}$ CPE_c) (R_{mt} C_{mt}). Subscript letters a and c indicate elements related to the anodic and cathodic sides respectively.

The charge transfer resistance $R_{ct,c}$ accounts for the adsorption of hydrogen on Pd and its subsequent reaction, e.g. HER (cathode side), while $R_{ct,a}$ is attributed to the hydrogen oxidation reaction (anode side). Both resistances get smaller as the cell voltage is made more negative, which is in agreement with an increase in the reaction kinetics of the anodic and cathodic reactions (cf. Figure 6(a, c)). As reported by Huth *et al.*,[39] the cell voltage has a far greater impact on the cathodic kinetics compared to the anodic ones, as the potential of the former is not clearly defined in the proton pump conditions. As already described in earlier paragraphs, the NPs size seems to have a direct influence on the reaction kinetics, with *Pd NPs "S"* showing a lower charge transfer resistance than *Pd NPs "M"* and *"L"* (Figure 6(a)). This result tends to show the opposite behaviour compared to Pd thin films, for which the charge transfer resistance increases with the decrease in thickness.[15,28] The difference could come from the surface defects and the crystal phases which may change with the NPs diameter, as well as the curvature of the Pd NPs, causing strain on the

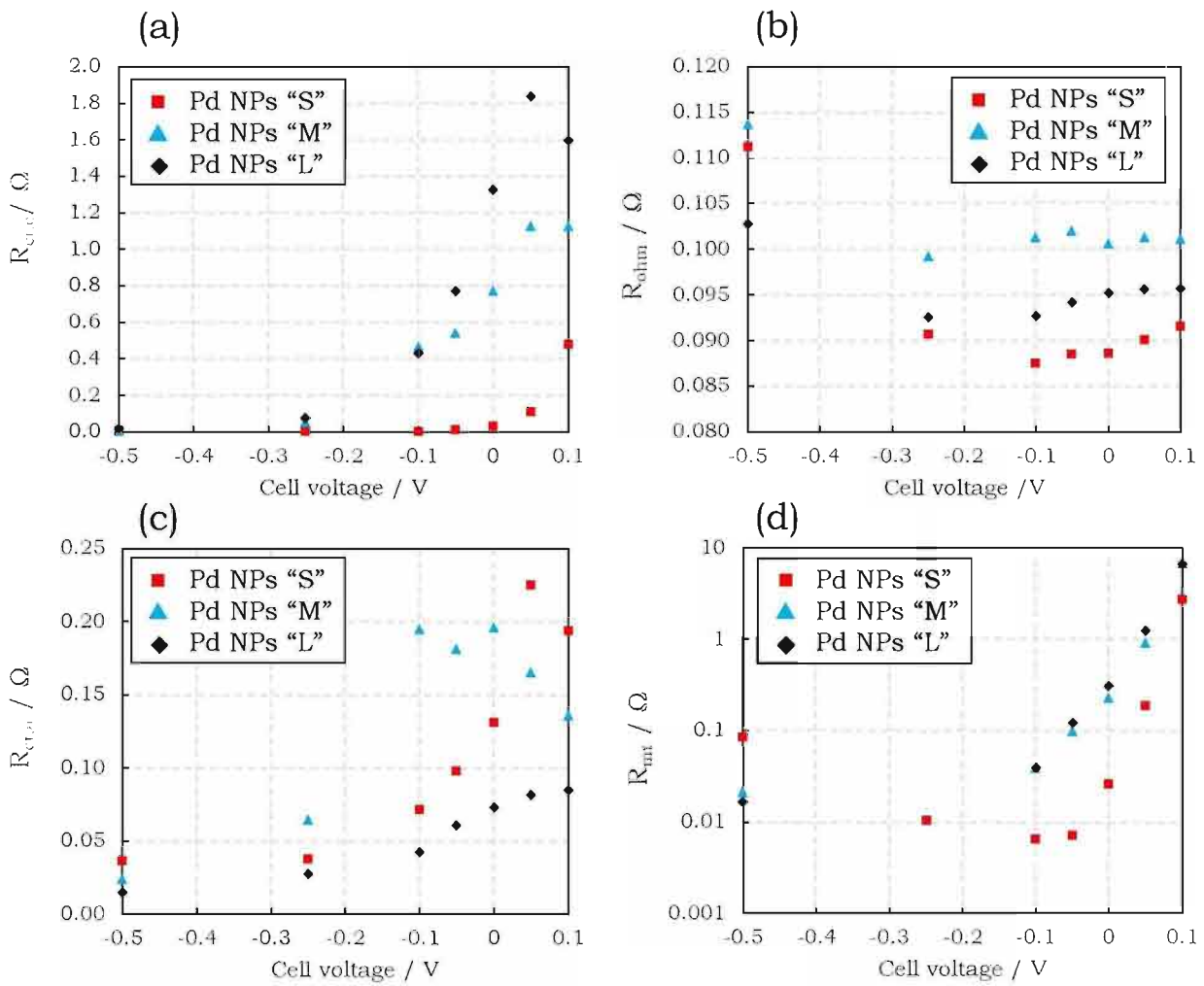

Figure 6. Voltage dependency of the cathodic charge transfer resistance (a), ohmic resistance (b), anodic charge transfer resistance (c), and mass transfer resistance (d) extracted from the modelling of the EIS data. H_2 and N_2 flowrates 50 mL min^{-1}, 30 °C, 20 min of stabilization at set potential, 20 mV fluctuations.

crystalline structure which might enhance the catalytic activity on the surface. Concerning the charge transfer on the anode side (Figure 6(c)), the differences appearing between the samples are likely due to the loading of Pt on the MEA. As a matter of fact, the Pt loading on the anodic side of the membrane is 0.36 mg cm^{-2}, 0.45 mg cm^{-2} and 0.58 mg cm^{-2} for *Pd NPs "S"*, *"M"*, and *"L"* respectively, which seems to correspond with the observed trend.

The ohmic resistance R_{ohm}, mainly attributed to the Nafion® membrane ionic resistivity, follows the same trend for all the samples (Figure 6(b)), the minor differences likely coming from slightly different membrane conditions, e.g. hydration or ageing. An increase of the ohmic resistance is always measured at low voltages, here below −0.25 V, likely due to the local dehydration of the membrane on the anodic side, as an increasing number of solvated protons depart from this side.[40]

The origin of the mass transfer resistance (Figure 6(d)) might be linked with (i) the diffusion of protons through the membrane to the cathode catalyst layer and (ii) the diffusion of H_2 to the anode catalyst layer (50 mL min^{-1}).

Three-electrode setup

Electrochemically active surface areas were measured from the integration of the PdO reduction peak located around 0.66 V_{RHE} (Figure 7(a)). As expected, the EASA decreases as the Pd particles are made larger, from 121 ± 6 cm^2 mgPd^{-1} for *Pd NPs Com*, to 8.2 ± 0.4 cm^2 mgPd^{-1} for *Pd NPs "L"* (cf. Table 2 for detailed values). These values are in the same range as the ones reported for Pt NPs synthesized in our group, between 20–60 cm^2 mg^{-1}.[42]

The kinetic rates for the HER and HOR were further examined in the three-electrode setup using potential sweeps, performed from 0.4 V_{RHE} to −0.05 V_{RHE}, at a scan rate of 2 mV s^{-1} (Figure 7(b)). The peak visible around 0.05 V_{RHE} is attributed to H

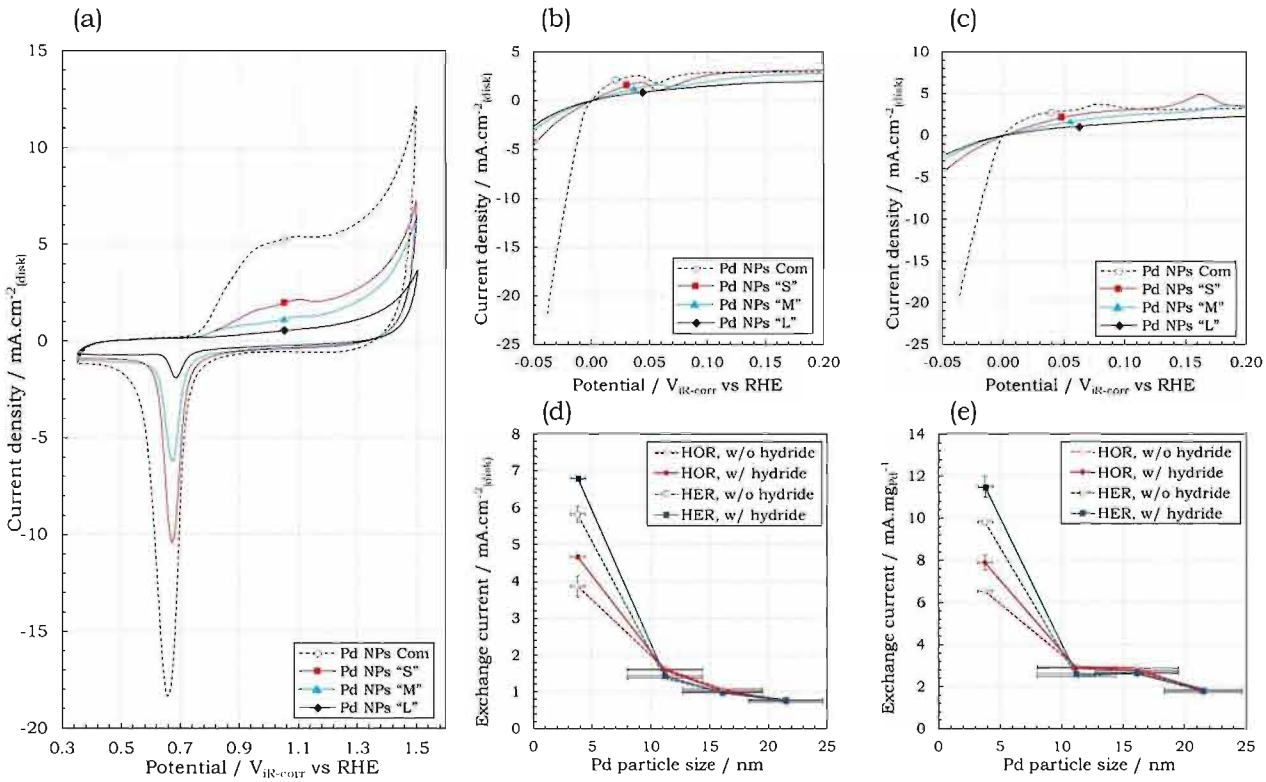

Figure 7. Cyclic voltammograms of the Pd materials recorded at 50 mV.s^{-1} (a). Linear sweep voltammograms recorded at 2 mV s^{-1} from 0.4 V_{RHE} to −0.05 V_{RHE} (negative scan, b) and from −0.05 V_{RHE} to 0.4 V_{RHE} (positive scan, c). Exchange currents dependency on the Pd particle diameter derived from the Butler-Volmer equation fitting (d, e). H_2SO_4 0.5 M, 25 °C, H_2 saturated electrolyte.

Table 2. Summary of the H insertion in Pd and kinetic parameters in the proton pump and three-electrode setup.

Sample ID	Proton pump H/Pd at −0.5 V	Onset potential at 10 mA mg$_{Pd}^{-1}$ (mV)	Three-electrode setup (RDE) H/Pd at −0.1 V_{RHE}	ECSA (cm^2 mg$_{Pd}^{-1}$)	i_0 HOR w/o hydrides (mA mg$_{Pd}^{-1}$)	i_0 HER w/o hydrides (mA mg$_{Pd}^{-1}$)	i_0 HOR w/ hydrides (mA mg$_{Pd}^{-1}$)	i_0 HER w/ hydrides (mA mg$_{Pd}^{-1}$)
Pd NPs Com	0.18	74	0.34	121 ± 6	6.52 ± 0.06	9.82 ± 0.11	7.88 ± 0.35	11.49 ± 0.48
Pd NPs "S"	0.32	56	0.41	56 ± 3	2.94 ± 0.06	2.48 ± 0.02	2.87 ± 0.05	2.59 ± 0.03
Pd NPs "M"	0.45	48	0.54	43 ± 2	2.89 ± 0.06	2.67 ± 0.03	2.76 ± 0.08	2.61 ± 0.04
Pd NPs "L"	0.56	41	0.63	8.2 ± 0.4	1.72 ± 0.10	1.85 ± 0.06	1.85 ± 0.06	1.79 ± 0.06

adsorption. The resulting curves were fitted with the Butler-Volmer equation, without constraining the α_{HOR} or α_{HER} parameters. Common values for α parameters were found between 0.2 and 0.4, which is close to the results from Zheng *et al.*, i.e. in the range of 0.3–0.45.[37] Detailed values are available in S.I. 5. The WE potential was iR corrected and additional potential deviation of the RHE electrode, ca. 1 mV, was also removed. The exchange current density i_0 is plotted versus the Pd particle diameter in Figure 7(d, e). As previously reported, the smaller the particles the higher the activity for both the HER and HOR. *Pd NPs Com* exhibits exchange currents as high as 6.52 ± 0.06 mA mg_{Pd}^{-1} and 9.81 ± 0.11 mA mg_{Pd}^{-1} for the HOR and HER respectively. The lowest values are recorded for *Pd NPs "L"*, displaying i_0 of 1.72 ± 0.10 mA mg_{Pd}^{-1} and 1.85 ± 0.06 mA mg_{Pd}^{-1} for the HOR and HER respectively. The reader is referred to Table 2 for further details, and to S.I. 5 for values relative to the surface area of Pd. A similar trend was observed by Zheng *et al.* for Pd NPs in the range of 3.2–33.6 nm in diameter.[37] When compared in terms of electroactive surface area, our values of i_0 are approximately 10–20 times lower than the ones reported by Zheng *et al.* or Durst *et al.* and 5 times lower than the values from Pronkin *et al.*[37,42,43] We attribute this difference to the material loading on the WE used in the present study, ca. 0.1 mg_{Pd}/cm^{-2}, which is greater than the one reported in these two studies, i.e. 5–15 $\mu g_{Pd}/cm^{-2}$.

The influence of Pd hydride on the HER and HOR was examined by reversing the direction of the potential sweep, from -0.05 V_{RHE} to 0.4 V_{RHE} (Figure 7(c)). After 60 s at -0.05 V_{RHE}, the Pd NPs should present a higher concentration of H atoms than when starting from 0.4 V. After fitting the LSV data, i_0 values were found to be close to the ones from the negative scans, apart from *Pd NPs Com* which presented a consistent increase in i_0 of about 20%. The lack of difference might come from the fact that even during the negative scans, a significant number of H atoms are inserted in the Pd structure starting from approximately 0.1 V_{RHE} (cf. Figure 4(a)). Additionally, the low scan rate may allow the PdH_x system to be in a quasi-equilibrium so that the H concentration is not considerably different between the positive and negative scans. The presence of a hysteresis in the H/Pd ratio measured for the commercial material (cf. Figure 4(a)) might explain the difference in i_0 for this sample.

Conclusion

Carbon black-supported palladium nanoparticles have been synthesized successfully in the range of 11.2–21.5 nm via a reverse micelle route, and their properties have been investigated along with a comparable commercial sample of 3.8 nm in diameter. Two experimental setups have been used: (i) a three-electrode setup with an acidic electrolyte (0.5 M H_2SO_4), and (ii) a proton pump setup with a proton exchange membrane. Despite being rarely employed in the literature, proton pumps allow unique investigations in a broad voltage range, i.e. up to -0.5 V in this paper, and bring insight into the behaviour of catalyst materials in a representative real application device.

The absorption of hydrogen into palladium has been explored as a function of the cell potential (or voltage) and the Pd NPs size. We report an increase in the number of H atoms interacting with Pd as the particle diameter is made larger, with H/Pd ratios ranging from 0.34 to 0.63 at -0.1 V_{RHE} in the three-electrode setup, and from 0.18 to 0.56 at -0.5 V in the PP. Overall, we evidenced a linear relationship between the maximum H/Pd and the Pd particle diameter in the range investigated. The electrochemical desorption curves were further analysed to separate the contributions coming from hydrogen absorption, adsorption, and oxidation. It was revealed that the concentration of H atoms on the Pd NPs surface does not necessarily increase with the surface area, i.e. with decreasing particle diameter, possibly due to a larger HER reaction rate. In addition to that, the kinetic of hydrogen insertion into Pd was studied in the PP, showing that increasing the Pd particle diameter extends the time necessary to reach an equilibrium, from approx. 3 s to 60–120 s for particles of 3.8 ± 0.6 nm and 21.5 ± 3.2 nm in diameter, respectively.

The HER and HOR kinetics have been studied in both setups. In the PP, the onset voltage for the HER evidenced a fall with the increase in particle diameter, from 74 mV to 41 mV at 10 mA mg_{Pd}^{-1}. This behaviour was supported by impedance measurements, which exhibited a significant increase in the charge transfer associated with the H adsorption along with the increase in particle diameter. A measurement of the exchange current densities was performed in the three-electrode setup. For the HOR, exchange currents ranged between 6.52 ± 0.06 mA mg_{Pd}^{-1} and 1.72 ± 0.10 mA mg_{Pd}^{-1} for particles of 3.8 ± 0.6 nm and 21.5 ± 3.2 nm in diameter, respectively. In the same diameter range, the HER exchange currents were found to be slightly higher, from 9.82 ± 0.11 mA mg_{Pd}^{-1} to 1.85 ± 0.06 mA mg_{Pd}^{-1}. In an attempt to determine the influence of hydrides on the reaction kinetics, we found that the smallest particles experience an increase in i_0 of about 20% when the potential is swept towards positive values compared to negative values, in the range of -0.05–0.4 V_{RHE}. This interesting result would deserve further investigation in the future.

Experimental

Synthesis of the palladium nanoparticles supported on Vulcan XC-72

The synthesis of the Pd NPs was performed following a two-microemulsion method. The procedure was inspired by ref.[30,31] and the details of the synthesis are available in S.I. 1. In brief, two microemulsions were prepared, containing either a Pd precursor ($Pd(NH_3)_4Cl_2$, 0.1 M) or a reducing agent (hydrazine hydrate, Sigma-Aldrich, approx. 64%), and both completed with a set quantity of surfactant (AOT, Sigma-Aldrich, $\geq$97%) and iso-octane (Sigma-Aldrich, $\geq$99%). After thorough stirring, the microemulsions are mixed together to yield Pd NPs. Finally, a carbon support is added to the mixture (Vulcan® XC-72, Cabot) before resolving the emulsion by adding THF. The material is then separated and

washed by centrifugation and dried overnight at 80 °C, before being calcinated at 250 °C for 2.5 h.

Palladium nanoparticles-based materials characterization

Transmission electron microscopy (TEM) observations were carried out with a JEOL JEM-2800. Samples were analysed in bright field mode with an acceleration voltage of 200 kV. The powders were first dispersed into ethanol (Etax Aa, Anora, >99.5 wt-%) and then deposited on holey carbon grids (AGS147-3, Agar Scientific).

Thermogravimetric analysis (TGA) was performed on a Q500 from TA Instruments under air. Approximately 5 mg of material was placed in an alumina crucible and inserted in the oven on a Pt alloy pan. Samples were heated up to 700 °C at 5 °C min^{-1}.

Preparation of the electrochemical setups

Inks containing the Pd NPs were prepared for the rotating disk electrode (RDE) and proton pump measurements. For the RDE, inks were prepared by mixing 5 mg of the catalyst material with 100 µL of milli-Q grade water (18.2 MΩ cm^{-1} at 25 °C), 100 µL of ethanol (Etax Aa, Anora, >99.5 wt-%) and 20 µL of a Nafion solution (Sigma-Aldrich, 5 wt-%). Then, 5 µL of ink was deposited on a glassy carbon tip (0.196 cm^2) and, once dried, the tip was soaked into hot electrolyte for about 1 min before fixing it to the rotating shaft to mitigate the hydrophobic nature of the catalyst layer. For the proton pump, inks were prepared by mixing 35.9 mg of the catalyst material, 71.9 µL of milli-Q water, 395 µL of iso-propanol (Honeywell, Chromasolv, ≥99.9 %) and 280 µL of a 5 wt-% Nafion solution. Membrane electrode assemblies (MEA) were prepared by spraying the catalyst ink on a 20 cm^2 Nafion membrane 115 (Ion Power), using a square pattern of 5.29 cm^2. The Pd-containing inks were sprayed as cathode catalysts, while the anode catalysts consisted of commercial Pt supported on carbon black (Alfa Aesar, 20 wt.%), prepared in the same conditions as the Pd-based inks. The metal loading on each side is approx. 0.5 $mg_{Me}\,cm^{-2}$ (Me = Pd or Pt). Finally, the MEAs were dried for 2 h at 180 °C in a vacuum oven (Heraeus) and stored in milli-Q water before further use.

The RDE setup was constituted of three electrodes introduced in a glass cell. The working electrode (WE) was placed on a rotator (Pine MSRX speed control), the counter electrode (CE) was an iridium wire, and the reference electrode (REF) was a reversible hydrogen electrode (RHE) (Gaskatel, Hydroflex®). The analyses were performed using an Autolab potentiostat (PGSTAT128 N) controlled by the software Nova. Measurements were carried out in 0.5 M H_2SO_4 electrolyte (Merck, Titripur®) at 25 °C. Nitrogen was bubbled for 30 min prior to the first measurement to ensure the removal of O_2 dissolved in the electrolyte.

The proton pump (PP) cell was based on a fuel cell (Fuel Cell Technology, Inc.), fed at the anode side with H_2 (AGA, 5.0), and at the cathode side with N_2 (AGA, 5.0), both humidified (100 %) before entering the cell. The gas pressure in the cell was equal to atmospheric pressure. Measurements were carried out with an Autolab potentiostat (PGSTAT100) and recorded with the software Nova. All the analyses were performed at 30 °C.

Electrochemical characterization procedures in the RDE setup

Electrochemically active surface area (ECSA) was determined based on the surface oxidation method. The measurements were carried out between 0.35–1.5 V_{RHE} at a scan rate of 50 $mV.s^{-1}$. The Pd reduction peak was integrated, and the resulting electric charge was converted into EASA assuming a charge for the reduction of a monolayer of PdO of 424 µC cm^{-2}.[32]

Hydrogen electrochemical loading and desorption measurements were carried out as follows. Hydrogen atoms are inserted into Pd at constant voltage/potential for 120 s. The desorption of H atoms is carried out at +0.4 V for 120 s. A small positive current (0.4–0.8 mA cm^{-2}) was always present during the desorption step in the PP due to the H_2 crossover through the Nafion membrane, resulting in its oxidation into protons. This contribution was removed by averaging this positive current during the last 10 s and subtracting it from the whole curve.

Potential controlled electrochemical impedance spectroscopy (EIS) was performed in both RDE and PP setups. In the RDE, EIS was carried out after 5 min of stabilization at 0.4 V_{RHE}, with a 10 mV amplitude in the frequency range from 100 kHz and 10 Hz (10 points per decade). In the PP, the measurements were performed after 20 min stabilization at the set voltage, using 20 mV amplitude in the frequency range from 10 kHz to 100 mHz.

The determination of the exchange current for the HER and HOR was done from the polarization curves in the region −0.05–0.4 V_{RHE}. After ensuring that the system is stable by performing 30 to 50 cyclic voltammetry (CV) in the same region at 25 $mV\,s^{-1}$, a potential of 0.4 V_{RHE} was applied to the WE for 60 s followed by a linear sweep of the potential starting from 0.4 V_{RHE} to −0.05 V_{RHE} at 2 $mV\,s^{-1}$. To study the influence of hydrides on the HER/HOR kinetics, additional sweeps were performed starting from −0.05 V_{RHE} and up to 0.4 V_{RHE}. The polarization curves were fitted with the Butler-Volmer equation (6) in the region −0.05–0.05 V_{RHE}.

$$i = i_0 \cdot \left(exp\left[\frac{\alpha_{HOR} F \eta}{RT}\right] - exp\left[\frac{\alpha_{HER} F \eta}{RT}\right] \right) \quad (6)$$

With i the current density, i_0 the exchange current density, α_{HER} (α_{HOR}) the cathodic (anodic) charge transfer coefficient, F the Faraday constant, T the absolute temperature, R the universal gas constant and η the overpotential. The applied potential was corrected from the ohmic losses, ca. 3–4 Ω, and the possible potential shift of the reference electrode, ca. 1 mV. The determination of i_0 and α coefficients was performed by minimizing the error (least squares) between the experimental data and the calculated data.

Supporting Information

Additional references cited within the Supporting Information.[44,45]

CRediT author statement

Lilian Moumaneix: Conceptualization, Methodology, Formal analysis, Investigation, Writing – Original Draft, Writing – Review & Editing, Visualization. **Akseli Rautakorpi**: Investigation, Writing – Review & Editing. **Tanja Kallio**: Conceptualization, Writing – Review & Editing, Supervision, Funding acquisition.

Acknowledgements

This project has received funding from the European Union's Horizon 2020 research and innovation program under grant agreement N° 952184 (the HERMES project).

Conflict of Interests

The authors declare no conflict of interest.

Data Availability Statement

The data used in the present study are available using the following link: https://doi.org/10.23729/46741a21-7a6f-42ad-af91-21624ebd4974

Keywords: Palladium · Reverse micelle synthesis · Proton pump · Hydrogen · HER HOR kinetics

[1] Z. W. Dunbar, *J. Power Sources* **2015**, *297*, 525–533.
[2] M. Yuan, K. Lee, D. G. Van Campen, S. Liguori, M. F. Toney, J. Wilcox, *Ind. Eng. Chem. Res.* **2019**, *58*, 926–934.
[3] I. Darmadi, F. A. A. Nugroho, C. Langhammer, *ACS Sens.* **2020**, *5*, 3306–3327.
[4] C. C. Ndaya, N. Javahiraly, A. Brioude, *Sensors* **2019**, *19*, 4478.
[5] S. Dekura, H. Kobayashi, K. Kusada, H. Kitagawa, *ChemPhysChem* **2019**, *20*, 1158–1176.
[6] D. Teschner, J. Borsodi, Z. Kis, L. Szentmiklósi, Z. Révay, A. Knop-Gericke, R. Schlögl, D. Torres, P. Sautet, *J. Phys. Chem. C* **2010**, *114*, 2293–2299.
[7] D. Teschner, J. Borsodi, A. Wootsh, Z. Révay, M. Hävecker, A. Knop-Gericke, S. D. Jackson, R. Schlögl, *Science* **2008**, *320*, 86–89.
[8] M. W. Tew, M. Nachtegaal, M. Janousch, T. Huthwelker, J. A. van Bokhoven, *Phys. Chem. Chem. Phys.* **2012**, *14*, 5761.
[9] S. F. Parker, H. C. Walker, S. K. Callear, E. Grünewald, T. Petzold, D. Wolf, K. Möbus, J. Adam, S. D. Wieland, M. Jiménez-Ruiz, P. W. Albers, *Chem. Sci.* **2019**, *10*, 480–489.
[10] B. M. Tackett, J. H. Lee, J. G. Chen, *Acc. Chem. Res.* **2020**, *53*, 1535–1544.
[11] Z. Wang, Z. Dai, S. Wang, H. Zhang, W. Tian, Y. Xu, X. Li, L. Wang, H. Wang, *Chem. Eng. J.* **2021**, *416*, 129105.
[12] W. Xu, G. Fan, J. Chen, J. Li, L. Zhang, S. Zhu, X. 5u, F. Cheng, J. Chen, *Angew. Chem. Int. Ed.* **2020**, *59*, 3511–3516.
[13] T. Skośkiewicz, *Phys. Status Solidi B* **1973**, *59*, 329–334.
[14] A. Czerwinski, I. Kiersztyn, M. Grden, J. Czapla, *J. Electroanal. Chem.* **1999**, *471*, 190–195.
[15] C. Gabrielli, P. P. Grand, A. Lasia, H. J. Perrot, *Electrochem. Soc. Interface* **2004**, *151*, A1925-A1936.
[16] S. M. Kozlov, H. A. Aleksandrov, K. M. Neyman, *J. Phys. Chem. C* **2014**, *118*, 15242–15250.
[17] G. Bambakidis, R. J. Smith, D. A. Otterson, *Phys. Rev.* **1969**, *177*, 1044–1048.
[18] S. Dekura, H. Kobayashi, R. Ikeda, M. Maesato, H. Yoshino, M. Ohba, T. Ishimoto, S. Kawaguchi, Y. Kubota, S. Yoshioka, S. Matsumura, T. Sugiyama, H. Kitagawa, *Angew. Chem.* **2018**, *130*, 9971–9975.
[19] E. Wicke, H. Brodowsky, H. Züchner in *Hydrogen in Metals II*, vol 29 (Eds.: G. Alefeld, J. Völkl), Springer, Berlin, Heidelberg, **1978**, 73–155.
[20] B. Ingham, M. F. Toney, S. C. Hendy, T. Cox, D. D. Fong, J. A. Eastman, P. H. Fuoss, K. J. Stevens, A. Lassesson, S. A. Brown, M. P. Ryan, *Phys. Rev. B* **2008**, *78*, 245408.
[21] F. A. Lewis, *Int. J. Hydrogen Energy* **1996**, *21*, 461–464.
[22] K. Hubkowska, M. Łukaszewski, A. Czerwiński, *Electrochim. Acta* **2010**, *56*, 235–242.
[23] L. Moumaneix, A. Rautakorpi, T. Kallio, *ChemElectroChem* **2023**, *10*, e202201109.
[24] J. D. Benck, A. Jackson, D. Young, D. Rettenwander, Y.-M. Chiang, *Chem. Mater.* **2019**, *31*, 4234–4245.
[25] R. P. Jansonius, P. A. Schauer, D. J. Dvorak, B. P. MacLeod, D. K. Fork, C. P. Berlinguette, *Angew. Chem. Int. Ed.* **2020**, *59*, 12192–12198.
[26] H. Duncan, A. Lasia, *Electrochim. Acta* **2007**, *52*, 6195–6205.
[27] P. N. Bartlett, B. Gollas, S. Guerin, J. Marwan, *Phys. Chem. Chem. Phys.* **2002**, *4*, 3835–3842.
[28] C. Gabrielli, P. P. Grand, A. Lasia, H. Perrot, *J. Electrochem. Soc.* **2004**, *151*, A1937-A1942.
[29] E. A. Crespo, S. Claramonte, M. Ruda, S. R. de Debiaggi, *Int. J. Hydrogen Energy* **2010**, *35*, 6037–6041.
[30] D.-H. Chen, C.-C. Wang, T.-C. Huang, *J. Colloid Interface Sci.* **1999**, *210*, 123–129.
[31] M. Chen, J. Falkner, W.-H. Guo, J.-Y. Zhang, C. Sayes, V. L. Colvin, *J. Colloid Interface Sci.* **2005**, *287*, 146–151.
[32] M. Łukaszewski, M. Soszko, A. Czerwinski, *Int. J. Electrochem. Sci.* **2016**, *11*, 4442–4469.
[33] N. A. Scholtus, W. Keith Hall, *J. Chem. Phys.* **1963**, *39*, 868–870.
[34] E. A. Owen, E. St J. Williams, *Proc. Phys. Soc.* **1944**, *56*, 52–63.
[35] W. Liu, Y. Magnin, D. Förster, J. Bourgon, T. Len, F. Morfin, L. Piccolo, H. Amara, C. Zlotea, *J. Mater. Chem. A* **2021**, *9*, 10354–10363.
[36] L. Birry, A. Lasia, *Electrochim. Acta* **2006**, *51*, 3356–3364.
[37] J. Zheng, S. Zhou, S. Gu, B. Xu, Y. J. Yan, *Electrochem. Soc. Interface* **2016**, *163*, F499–F506.
[38] B. A. Boukamp, Equivalent circuit users manual, 2nd revised edition, Department of Chemistry, Technical University of Twente, **1989**.
[39] A. Huth, B. Schaar, T. Oekermann, *Electrochim. Acta* **2009**, *54*, 2774–2780.
[40] M.-T. Nguyen, S. A. Grigoriev, A. A. Kalinnikov, A. A. Filippov, P. Millet, V. N. Fateev, *J. Appl. Electrochem.* **2011**, *41*, 1033–1042.
[41] T. Rajala, R. Kronberg, R. Backhouse, M. E. M. Buan, M. Tripathi, A. Zitolo, H. Jiang, K. Laasonen, T. Susi, F. Jaouen, T. Kallio, *Appl. Catal. B* **2020**, *265*, 118582.
[42] J. Durst, C. Simon, F. Hasché, H. A. Gasteiger, *J. Electrochem. Soc.* **2015**, *162*, F190–F203.
[43] S. N. Pronkin, A. Bonnefont, P. S. Ruvinskiy, E. R. Savinova, *Electrochim. Acta* **2010**, *55*, 3312–3323.
[44] D.-H. Chen, C.-C. Wang, T.-C. Huang, *J. Colloid Interface Sci.* **1999**, *210*, 123–129.
[45] M. Chen, J. Falkner, W.-H. Guo, J.-Y. Zhang, C. Sayes, V. L. Colvin, *J. Colloid Interface Sci.* **2005**, *287*, 146–151.

Manuscript received: March 8, 2023
Revised manuscript received: May 9, 2023
Version of record online: June 26, 2023